

Large- k exciton dynamics in GaN epilayers: Nonthermal and thermal regimes

Anna Vinattieri*

Dipartimento di Fisica e Astronomia, LENS, CNISM, Università di Firenze, Italy

Franco Bogani

*Dipartimento di Energetica, Università di Firenze, Italy*Lucia Cavigli,[†] Donatella Manzi, and Massimo Gurioli*Dipartimento di Fisica e Astronomia, CNISM, LENS, Università di Firenze, Italy*

Eric Feltin, Jean-François Carlin, Denis Martin, Raphaël Butté, and Nicolas Grandjean

Institute of Condensed Matter Physics, Ecole Polytechnique Fédérale de Lausanne, CH-1015 Lausanne, Switzerland

(Received 5 November 2012; revised manuscript received 22 January 2013; published 7 February 2013)

We present a detailed investigation performed at low temperature ($T < 50$ K) concerning the exciton dynamics in GaN epilayers grown on c -plane sapphire substrates, focusing on the exciton formation and the transition from the nonthermal to the thermal regime. The time-resolved kinetics of longitudinal-optical-phonon replicas is used to address the energy relaxation in the excitonic band. From picosecond time-resolved spectra, we bring evidence for a long lasting nonthermal excitonic distribution, which accounts for the first 50 ps. Such a behavior is confirmed in different experimental conditions when both nonresonant and resonant excitations are used. At low excitation power density, the exciton formation and their subsequent thermalization are dominated by impurity scattering rather than by acoustic phonon scattering. The estimate of the average energy of the excitons as a function of delay after the excitation pulse provides information on the relaxation time, which describes the evolution of the exciton population to the thermal regime.

DOI: [10.1103/PhysRevB.87.075202](https://doi.org/10.1103/PhysRevB.87.075202)

PACS number(s): 78.30.Fs, 78.55.Cr, 78.47.jd, 71.35.Cc

I. INTRODUCTION

In direct band gap semiconductors, the presence of excitonic resonances in optical spectra is considered as a clear marker to assess the sample quality. In the paradigmatic GaAs-based systems, excitons are usually probed by means of photoluminescence (PL) experiments, and their dynamics is investigated in a restricted wave-vector (k) interval near the Γ point (close to $k = 0$) as a consequence of the radiative recombination process, which requires, in the photon emission, both energy and momentum conservation. Therefore, when an excess energy is used to excite the sample, the rise time of the PL signal at the exciton energy includes all the information concerning exciton formation and their relaxation towards the $k \approx 0$ radiative states, making difficult to extract quantitative information on each process. Even when resonant excitation is used, the information on the $k \neq 0$ excitons can only be obtained by a careful modeling of the exciton dynamics.¹ For semiconductors where excitons strongly interact with the lattice, phonon replicas (PR) of the $k = 0$ excitonic band [the so-called zero-phonon line (ZPL)] are present in the PL spectra. Two possible situations can occur depending on the exciton localization/delocalization process in the material.

In disordered/defective materials—where most of the recombinations come from extrinsic contributions—excitons are strongly localized. The Huang-Rhys (HR) model is then commonly used to describe the replica characteristics and to extract the HR coefficient, which quantifies the exciton interaction with the lattice. This has been extensively done in III-nitrides both in epilayers and quantum confined heterostructures.^{2–4} In this case, the phonon-assisted transitions “replicate” the

ZPL shape and contain the same information on the exciton localization dynamics. Depending on the localization degree, a thermal regime can eventually be reached, which requires tens or hundreds of picoseconds.

On the other hand, in samples where exciton localization is weak, the free exciton (FE) thermalization issue is relevant, and from the study of the phonon-replica emission, we can expect extracting useful information on the exciton distribution over an extended k range. Moreover, even if the ZPL shows bound exciton emission [in nonintentionally doped (nid) GaN epilayers, excitons are mainly bound to donor states], the PR bands mostly originate from intrinsic excitonic states, making negligible the contribution of the extrinsic band. The PR bands contain information on the whole ($k = 0$ and $k \neq 0$) exciton population, since the momentum conservation rule is assured by the presence of one or more phonons. In particular, longitudinal optical (LO) phonons, of energy E_{LO} , are very effective in determining intense PR-PL bands, which are denominated n LO bands depending on the number n of LO phonons involved in the emission process. In fact, it has been shown that the shape of the 2LO PR of the FE band is proportional to the FE population, while the 1LO PR of the FE band reflects the FE population times the exciton kinetic energy.⁵

Therefore phonon replicas have been investigated in different semiconductors to assess both the exciton-phonon interaction and the FE dynamics at large k , which are of interest not only for fundamental physics studies but also for applications.⁶ In particular, the study of the phonon-assisted radiative recombinations provides significant information on the exciton dynamics in II-VI and III-V nitride semiconductors,

which show pronounced phonon-assisted emission.⁷ In III-V nitride structures, most of the reports on PR refer to the steady-state regime.^{8,9} We recently showed¹⁰ that a close comparison with existing models⁵ for the PR emission in GaN epilayers is relevant provided a free exciton thermalized distribution is achieved and taking into account the complex nature of the exciton band in GaN. In this way, a full reconstruction of the exciton density of states is made possible and the experimental PR energy shift, lineshape, and intensity are nicely reproduced by this model.

The $k = 0$ exciton dynamics in GaN epilayers has been extensively investigated both at the femtosecond and picosecond time scale. Typically, a 150-ps radiative recombination time and fast dephasing times (equal to 1–2 ps in high-quality samples at low excitation density) are found for the A and B excitons.^{11–13} Nevertheless, despite the fact that in the 1–100-ps range, the exciton dynamics is dominated by large- k excitons, the PR recombination kinetics has been scarcely investigated mainly focusing on the quasithermal regime.¹⁴ But even if the exciton-acoustic phonon interaction is quite strong, the thermal regime is reached after a finite time. This implies the presence of a nonthermal regime, which has not been experimentally investigated yet. Only theoretical results concerning the exciton formation and their relaxation to thermal equilibrium are reported in the literature.^{15–17}

In this study, we aim at filling this gap, and therefore we explore both the nonthermal and the thermal regimes. From picosecond time-resolved experiments performed on *ni*d GaN epilayers grown on *c*-plane sapphire substrates, we show that the achievement of a hot thermal distribution of excitons requires a few tens of picoseconds, depending on the excitation energy, the lattice temperature, and the excitation power density. The heating process is also studied by resonantly exciting the $k = 0$ FE (X_A exciton). As a consequence of the different wave-vector intervals explored by the PR and the ZPL emissions, we provide insights on the exciton dynamics in an extended region near the Γ point of the first Brillouin zone.

II. EXPERIMENTAL

The investigated samples are an 11- μm thick *ni*d wurtzite GaN epilayer grown by hydride vapor phase epitaxy (HVPE) on a *c*-plane sapphire substrate¹⁸ (sample A) and a 3- μm thick *ni*d wurtzite GaN epilayer grown by metal organic vapor phase epitaxy (MOVPE) on a *c*-plane sapphire substrate (sample B). The threading dislocation density is as low as $2 \times 10^8 \text{ cm}^{-2}$ in the HVPE sample and lower than $1 \times 10^9 \text{ cm}^{-2}$ in the MOVPE epilayer with a nonintentional *n*-type doping $\approx 10^{17} \text{ cm}^{-3}$ for the MOVPE sample and $\approx 3 \times 10^{17} \text{ cm}^{-3}$ for the HVPE one.

Measurements were performed with the sample placed in a closed-cycle cryostat varying the temperature from 10 to 50 K for time-resolved experiments. Reflectivity measurements at normal incidence were carried out using a cw Xe lamp. Time-integrated photoluminescence (TI-PL) measurements were performed under nonresonant excitation with a frequency-doubled picosecond dye laser emitting at 300 nm, and the collected light was detected by a cooled silicon charge coupled device camera after dispersion through a 50-cm flat-field spectrometer with a spectral resolution of 1 meV. Time-resolved

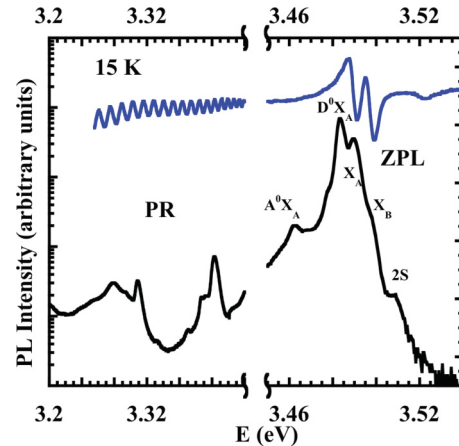


FIG. 1. (Color online) PL and reflectivity spectrum measured at 15 K showing the details of the ZPL and phonon replica (PR) bands.

photoluminescence (TR-PL) measurements were performed using a frequency-doubled mode-locked Ti:sapphire laser pumped by a continuous wave Ar⁺ laser providing 1.2-ps pulses at a repetition rate of 81 MHz. The PL was dispersed through a 30-cm flat-field monochromator and detected by a streak camera apparatus with a 3-ps time resolution.

In Fig. 1, typical TI-PL spectra taken at $T = 15$ K for the ZPL and the PR region are shown for sample A. Similar spectra for sample B are shown in Ref. 10. The main spectral features observed in the ZPL region at 10 K are related to the neutral donor-bound exciton recombination (D^0X_A) and to the X_A and X_B exciton radiative recombinations. The emission from the 2S state of X_A excitons is also detected at higher energy. The reflectivity spectrum (blue line in Fig. 1) shows clear excitonic resonances confirming the labeling of the PL structures. In this case, the X_C excitonic resonance is detected at ~ 3.52 eV. In the PR region, the reflectivity spectrum shows only interference fringes related to the epilayer thickness. From the comparison of Fig. 1 and the spectra reported in Ref. 10, it turns out that samples A and B show very similar features and pronounced excitonic resonances. The measured Stokes shift for the X_A exciton, detected at 15 K, is also very similar and is lower than 1.5 meV in both samples indicating a weak exciton localization at low T . The difference observed in the exciton energies, as extracted from the reflectivity spectra, comes from the different residual biaxial strains of the two epilayers and agrees with data and calculations already published.^{19,20} For a detailed discussion on the TI-PL spectra, we refer the readers to Ref. 10. We only mention that the TI-PL line shape almost coincides with the long-delay TR-PL line shape and that it agrees well with the thermal model of Segall and Mahan⁵ when the discrepancy commonly reported for the temperature behavior of the phonon replicas is described by accounting for the complexity of the GaN excitonic band.¹⁰

Here, we will focus on the time-resolved spectra to investigate the typical time scale for reaching a quasithermal distribution for which the model of Ref. 5 can be applied. Since the experimental results turn out to be very similar for samples A and B, most of the data we will show hereafter will refer to sample A.

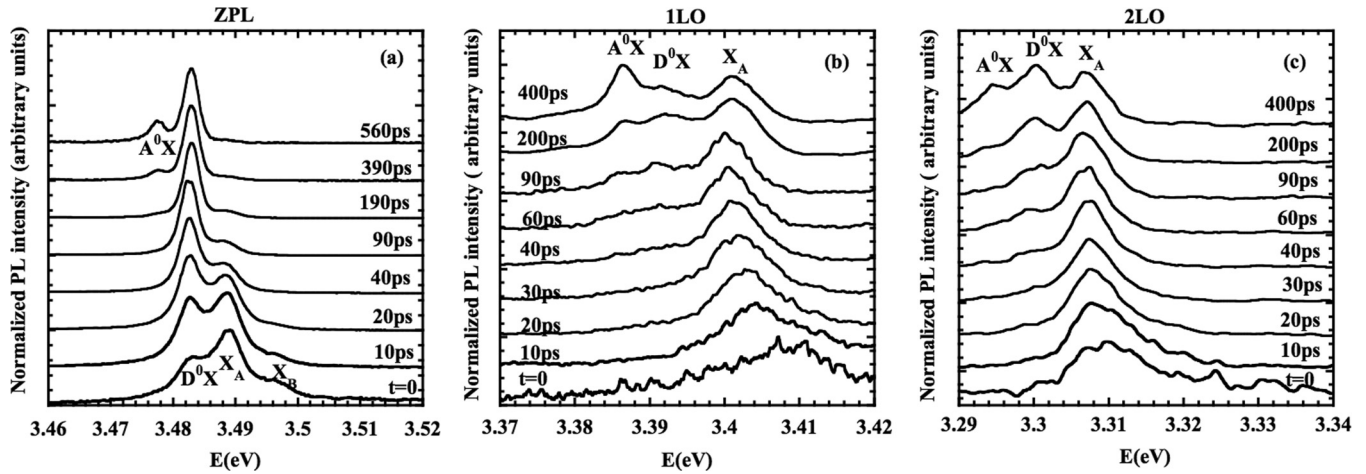


FIG. 2. TR spectra of the (a) ZPL, (b) 1LO-phonon, and (c) 2LO-phonon replica measured for different delay times after the excitation. The maximum of each spectrum is normalized to unity and spectra are vertically shifted for clarity.

In Fig. 2, typical TR-spectra are shown for (a) the ZPL, (b) the first LO phonon replica (1LO), and (c) the second LO phonon replica (2LO) acquired when exciting the sample with 3.55 eV photons (i.e., photons with an excess energy of nearly 60 and 35 meV with respect to the bottom of the exciton and free carrier bands, respectively, which is, however, still lower than the energy $E_{LO} = 92$ meV of the dominant LO phonon). Here and in the following, the zero delay time corresponds to the maximum of the excitation pulse as measured from the Rayleigh or Raman scattered light. It appears that for the ZPL, most of the dynamics involving free exciton states, both A and B ones, occurs during the first 40 ps following the excitation. The modifications seen at later times in the ZPL line shape come from the increasing contribution of the donor- and acceptor-bound exciton states. Concerning the time evolution of the replica bands, we will first focus on the 2LO-phonon band whose shape and intensity is directly proportional to the population of the exciton k states.⁵ At early times, the emission is blue shifted and broadened with respect to that measured at delays longer than 100 ps. Besides, for delays longer than 40 ps, the spectrum gets narrower and shifts to the energy position expected for a thermal exciton population.

The complexity of the exciton dynamics, which involves a nonthermal and a quasithermal regime at the picosecond time scale, is suggested by the different time evolutions of the spectral components of the 2LO-phonon band reported in Figs. 3(a) and 3(b), respectively. As a general trend, the rise and fall times get shorter with increasing energy of the recombining state. The rise time of the high-energy states (where only FE are present), at the limit of our experimental time resolution, indicates an exciton-formation time ≈ 10 ps followed by a PL decay occurring on a 100-ps time scale, which originates from both the population thermalization and decay. At early times, the high-energy side of the phonon replica is faster than the X_A emission, and we recover a common exponential decay at longer delays, indicating the establishment of the thermal regime. The lower-energy states exhibit a slower rise and decay as a consequence of the population dynamics and/or the exciton cooling. In Fig. 3(c), we show the time evolution

of the spectrally integrated free exciton emission of the 2LO-phonon band, excited with an excess energy of ≈ 60 meV for two different power densities (10 and 100 W cm^{-2}) normalized to the excitation power density. The fit with an exponential rise and decay is reported in the experimental data and, for clarity, the experimental time response is also shown. In this case, the rise and decay times reflect the time evolution of the total exciton population unaffected by thermalization, which only produces a redistribution of excitons in different k states. In the following, we will refer to the rise time of the spectrally integrated PL as to the “exciton-formation time.” Figure 3(c) clearly shows a decrease in the exciton formation time (and a 20% superlinearity) when increasing the excitation power density from 10 to 100 W cm^{-2} . In addition, the exciton-formation time only slightly depends on the excitation energy as supported by the decrease from 13 to 9 ps when reducing the excitation excess energy below the free carrier absorption edge (from 60 to 20 meV with respect to the bottom of the exciton band). This suggests, as we will discuss later, that we mostly create electron-hole (e-h) correlated pairs rather than free carriers, even when we excite the samples a few tens of milli-electron-volts above the free carrier continuum.

Let us now move to the study of the exciton relaxation process. In Fig. 4, we show the comparison between the 2LO phonon replica time-resolved spectra taken at $t = 10$ and 114 ps delay time after the excitation pulse. It is worth pointing out that the overall exciton dynamics is almost independent of the excess energy of the exciting photons (not shown here); therefore in the following, the experimental data will refer to the excitation energy of 3.55 eV. The exciton relaxation dynamics has been commonly interpreted as a cooling process assuming that an exciton thermal distribution can be reached within a few picoseconds^{14,21} and then that the PL lineshape can be reproduced with a Boltzmann distribution with a temperature that depends on the delay time. In fact, in agreement with previous reports,¹⁴ we find that, within the experimental sensitivity, the high-energy tail of the emission is mostly exponential even at very short delay times. However, we can perform a more accurate analysis by using the fact that

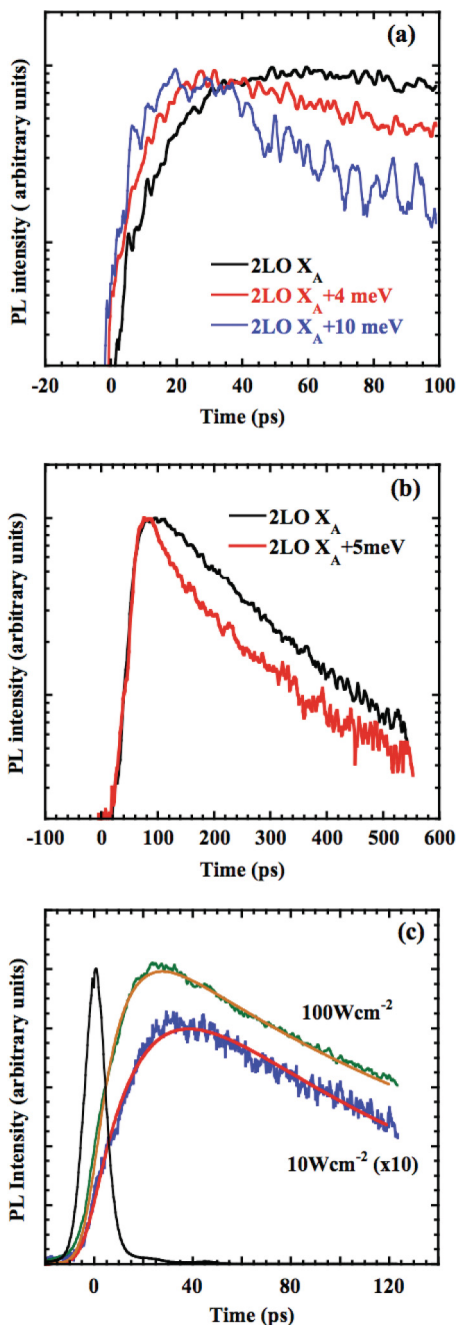


FIG. 3. (Color online) PL time evolution measured at different energies around the 2LO-phonon X_A exciton (a) in a restricted and (b) over an extended time scales. (c) Time evolution of the spectrally integrated emission of the 2LO-phonon band (including only the free exciton contribution from 3.304 to 3.33 eV) for two different excitation power densities (10 and 100 W cm⁻²). Orange and red lines are fits as discussed in the text. The black line is the experimental time response.

the line shape of the 2LO-phonon band is directly related to the population within the exciton band by

$$I_{2LO}(E, t) \propto \rho(\epsilon) f(\epsilon, t) \Theta(\epsilon), \quad (1)$$

where $\epsilon = (E - E_0)$ is the exciton kinetic energy, $E_0 = E_{X_A} - 2E_{LO}$, $\rho(\epsilon)$ represents the exciton density of states, $f(\epsilon, t)$ is the exciton distribution function at time t , and Θ is

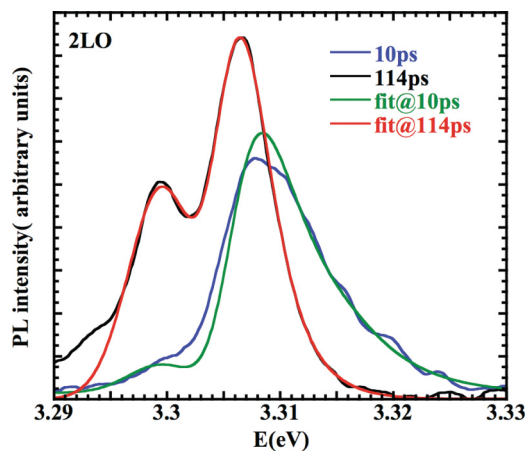


FIG. 4. (Color online) TR spectra of the 2LO-phonon band at different delays along with a fit as discussed in the text.

the Heaviside function.⁵ Generally speaking, $f(\epsilon, t)$ can even be a nonthermal distribution and, in fact, reasonable fits to the time-resolved 2LO-phonon emission spectra using Boltzmann function for $f(\epsilon, t)$ are only obtained at long delays. In Fig. 4, we compare the time-resolved 2LO-phonon spectra with the corresponding fits using a Boltzmann-like distribution. The spectrum at a delay time of 114 ps is nicely reproduced by $\rho(\epsilon)$ given in Ref. 10 and $k_B T_L = 1.97$ meV, T_L being the temperature of the lattice. The best fit to the data at a delay time of 10 ps requires a hotter thermal distribution ($k_B T = 3.77$ meV). However, the quality of the fit is poorer. In particular, the states near the peak energy reveal a lack of population with respect to the thermal condition, suggesting a nonthermal exciton distribution.

In order to quantitatively discuss the exciton thermalization, first of all, we normalize each time-resolved spectrum of the 2LO-phonon PL band with its spectrally integrated intensity. This operation eliminates the exciton formation and recombination from the line-shape analysis, which, to a first approximation, only affects the total number of excitons. The resulting normalized spectra $I_{2LO}^*(E, t)$ is then proportional to the normalized exciton population $N(E, t)$. In Figs. 5(a) and 5(b), we report the time evolution of the normalized spectra $I_{2LO}^*(E, t) \propto N(E, t)$ at fixed energies for two different excitation power densities (10 and 100 W cm⁻²). The quantity $N(E, t)$ decreases with time for large E values, while it increases for small E values. These trends are obviously associated with the transfer of population towards the bottom of the excitonic band. We also observe that the state of energy around 3.310 eV, nearly corresponding to an excess of energy $3k_B T_L/2$ above the bottom of the exciton band, rapidly reaches the equilibrium value at temperature T_L , i.e., a constant value of the population. A faster thermalization is observed at higher excitation power density, as expected if we take into account exciton-exciton interaction.

The next step is to bypass the problem of modeling $\rho(\epsilon)$. To this aim, considering the ratio $n(E, t) = I_{2LO}^*(E, t)/I_{2LO}^*(E, t = 200 \text{ ps})$ between the normalized spectra, we have experimental data that do not depend on the actual $\rho(\epsilon)$. In fact, according to the experimental data, we can assume a thermal distribution at the lattice temperature

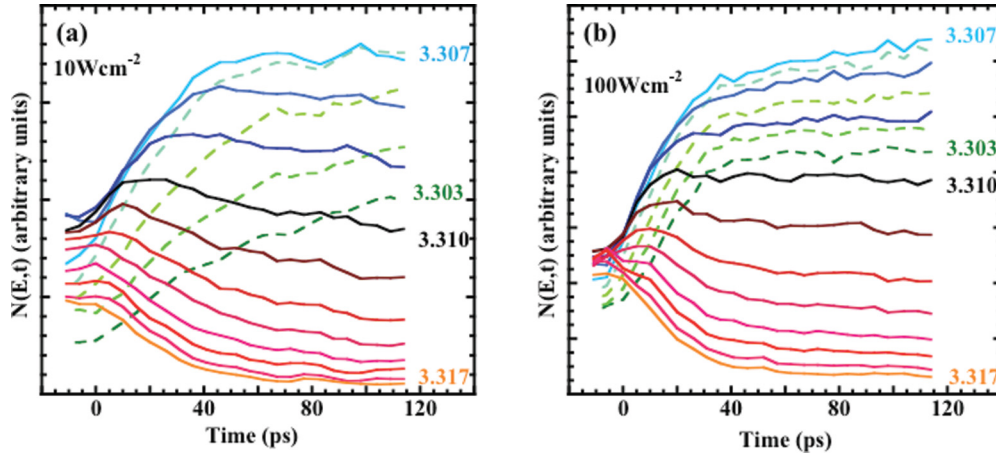


FIG. 5. (Color online) Time evolution of the normalized exciton population $N(E,t)$ at different energies (equispaced) in the 2LO band for (a) 10 and (b) 100 W cm^{-2} excitation power densities. The continuous (dashed) lines refer to states lying above (below) 3.307 eV.

for $t > 100 \text{ ps}$ (hereafter $t = \infty$). Then, from Eq. (1), the 2LO-phonon normalized emission band at $t = \infty$ is given by

$$I_{2\text{LO}}^*(E, \infty) \propto \frac{\rho(\epsilon) e^{-\frac{\epsilon}{k_B T_L}}}{(k_B T_L)^{(3/2)}} \Theta(\epsilon), \quad (2)$$

and therefore from $n(E,t)$, we can extract the exciton distribution $f(\epsilon,t)$ even if the density of states is unknown.

In order to get more direct information on the exciton distribution $f(\epsilon,t)$, we define the quantity $\beta^*(E,t)$:

$$\begin{aligned} \beta^*(E,t) &= \ln \frac{I_{2\text{LO}}^*(E,t)}{I_{2\text{LO}}^*(E,\infty)} \\ &= \ln[(k_B T_L)^{(3/2)} f(\epsilon,t)] + \frac{\epsilon}{k_B T_L}. \end{aligned} \quad (3)$$

$\beta^*(E,t)$ turns out to be an indicator of the degree of thermalization of the excitons and it is independent of the actual density of states. Whenever the hot-exciton picture applies, i.e., when the exciton distribution $f(\epsilon,t)$ is a quasithermal distribution with a time-dependent temperature $T(t)$, we get

$$\beta^*(E,t)_{\text{th}} = \epsilon \left[\frac{1}{k_B T_L} - \frac{1}{k_B T(t)} \right] + \frac{3}{2} \ln \left[\frac{k_B T_L}{k_B T(t)} \right]. \quad (4)$$

In the hot-exciton limit, we therefore expect to get a straight line, at fixed time, when plotting $\beta^*(E,t)$ as a function of energy with a slope given by $[\frac{1}{k_B T_L} - \frac{1}{k_B T(t)}]$. Any deviation from a linear dependence versus E is therefore a signature for a nonthermal regime.

In Fig. 6(a), $\beta^*(E,t)$ is reported for different delay times, in the 2LO-phonon spectral region, as extracted from TR spectra. The nominal lattice temperature is equal to 10 K and the sample is excited with an excess energy of $\approx 60 \text{ meV}$ with respect to E_{X_A} with a power density of 10 W cm^{-2} . For clarity, we report the value of $\beta^*(E,t)$ only in the spectral region of the free exciton emission with the low-energy side cutoff corresponding to the onset of the 2LO-phonon D^0X_A emission. In this figure, the energy E is identified with the photon emission energy and not only the kinetic energy term. We also show the time-integrated PL spectrum of the 2LO-phonon replica corresponding to the full thermal regime. Strong deviations from a linear trend of $\beta^*(E,t)$ over the whole 2LO-free exciton

band (3.304–3.33 eV) are observed at the early stage of the exciton dynamics ($t < 40 \text{ ps}$). In particular, the flattening of $\beta^*(E,t)$ in the low-energy side (3.303–3.308 eV) comes from a lack of population with respect to a quasithermal distribution.

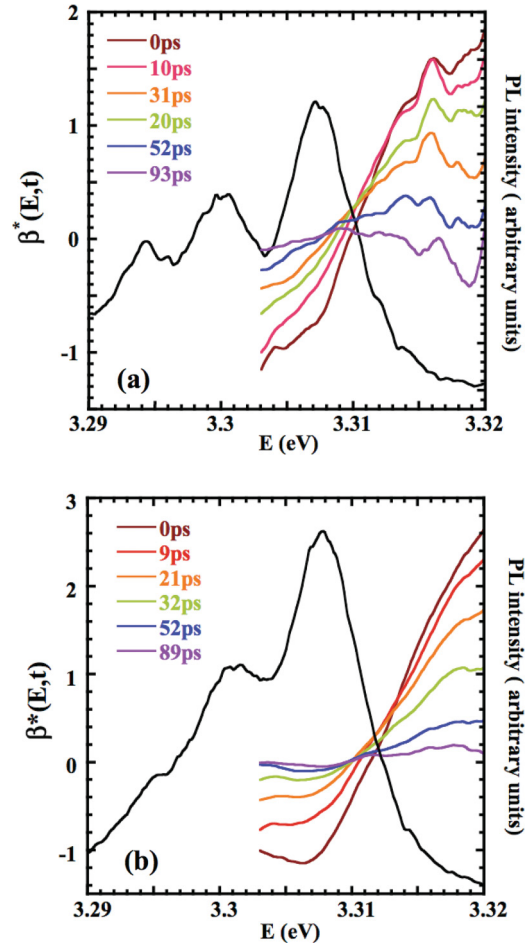


FIG. 6. (Color online) Time evolution of the quantity $\beta^*(E,t)$ for different delay times for nonresonant excitation: (a) 10 and (b) 100 W cm^{-2} . The solid black line in (a) and (b) is the time-integrated PL spectrum.

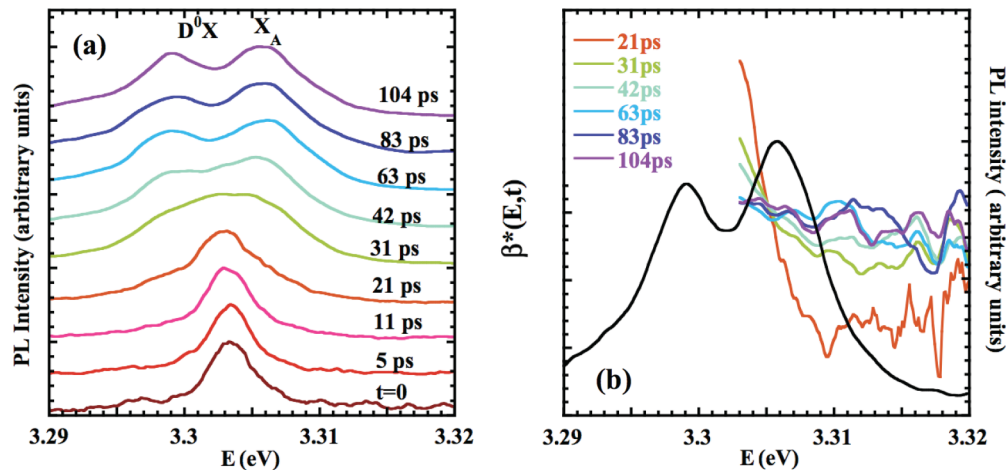


FIG. 7. (Color online) (a) Time-resolved spectra taken at different delay times for resonant excitation. (b) Time evolution of the quantity $\beta^*(E, t)$ for the resonant case. For clarity, the 2LO-phonon PL spectrum in the fully thermalized regime is also shown (black solid line).

We also observe a flattening of $\beta^*(E, t)$ on the high-energy side (corresponding to the tail of the PL band), which could be a further indication for a nonthermal distribution. However, this part of the spectra (for $E \gtrsim 3.315$ eV), where the PL intensity is low, is affected by a relevant background whose subtraction is delicate making reliable conclusions rather hazardous. On the contrary, the value of $\beta^*(E, t)$ on the low-energy side (where the PL intensity is high) is affected by a small error (a few percent). It turns out that, only at longer delays ($t > 50$ ps), the distribution function behaves like a Boltzmann function and $\beta^*(E, t)$ shows a linear dependence over the whole energy range covered by the 2LO-phonon band with a decreasing slope in agreement with a cooling of the exciton population. Finally, $\beta^*(E, t)$ becomes constant and vanishes, as expected, when the distribution reaches the lattice temperature. Referring to Fig. 6(a), the deviation of $\beta^*(E, t)$ from the linear behavior observed for $t < 40$ ps indicates the lack of excitonic population not only with respect to the thermal regime at $T = T_L$ but also with respect to a hot-exciton distribution.

Therefore our findings clearly evidence the presence of a nonthermal distribution of the exciton population at short delay times. It comes out that the cooling picture of a hot-exciton distribution does not apply if we refer to the whole excitonic band.

Moreover, the lack of population at the X_A energy with respect to the hot thermal distribution cannot be ascribed to a localization mechanism. In fact, the absence of any significant localization of the excitons is proved by the comparison of reflectivity and PL spectra for the ZPL (see Fig. 1) where it turns out that the Stokes shift at 10 K is ≈ 1 meV, a value not large enough to explain the experimental results displayed in Fig. 6(a). In Fig. 6(b), similar spectra are reported for an excitation power density of 100 W cm^{-2} . No major change is found except that the quasithermal regime is reached for slightly shorter times with respect to the low-excitation condition, as already shown in Fig. 5. Up to 50 K, the nonthermal regime can still be detected during the first 30 ps and similar results for $\beta^*(E, t)$ are observed when we change the photon excitation energy for an excess energy lying in the 6 to 60 meV range.

An opposite behavior (i.e., heating instead of cooling) is instead observed when we resonantly excite the $k = 0$ X_A exciton and we study the heating of the corresponding exciton distribution. In Fig. 7(a), TR spectra are shown for different delay times after resonant excitation at $E = 3.303$ eV slightly below the X_A exciton energy. Apart from the initial Raman signal detected for the first 10 ps (peak in the figure), which dominates the emission spectra at the early stage, the exciton line and also that of the D^0X_A emission are visible at $t \geq 20$ ps. In Fig. 7(b), we report $\beta^*(E, t)$ for $t \geq 20$ ps when the Raman signal can be neglected and we can discuss the evolution of the exciton distribution without spurious emission. Due to this cut occurring at the early stage in the time evolution of the excitons, it is not possible to have a definitive proof of their nonthermal distribution under this excitation condition. Still $\beta^*(E, t)$ shows a slope opposite to that reported for nonresonant excitation in the spectral region 3.303–3.310 eV, denoting a cold exciton distribution. During the thermalization process, we observe an exciton heating with a population transfer between low- and high-energy states until the equilibrium distribution at temperature T_L is reached. Quite remarkably, we find that the time scale for reaching the equilibrium distribution is almost the same for the cooling and heating of the exciton population. Finally, it is worth noting that, when comparing the PL spectra shown in Figs. 6 and 7, a saturation of the acceptor emission is observed (see Fig. 6) when increasing the excitation power density while it is its absence, which is observed when exciting the sample resonantly (see Fig. 7).

III. DISCUSSION

The analysis of the 2LO PR-PL line shape, without any supplementary modeling of the exciton density of states, already gives important information on the excitonic distribution function. However, to quantitatively study the thermalization process, we have to analyze and compare the time evolution of the mean energy $\langle \epsilon(t) \rangle$ and that of the effective temperature $T(t)$ of the exciton distribution.

$\langle \epsilon(t) \rangle$ can be directly obtained from the experimental data by considering the ratio between the spectrally integrated

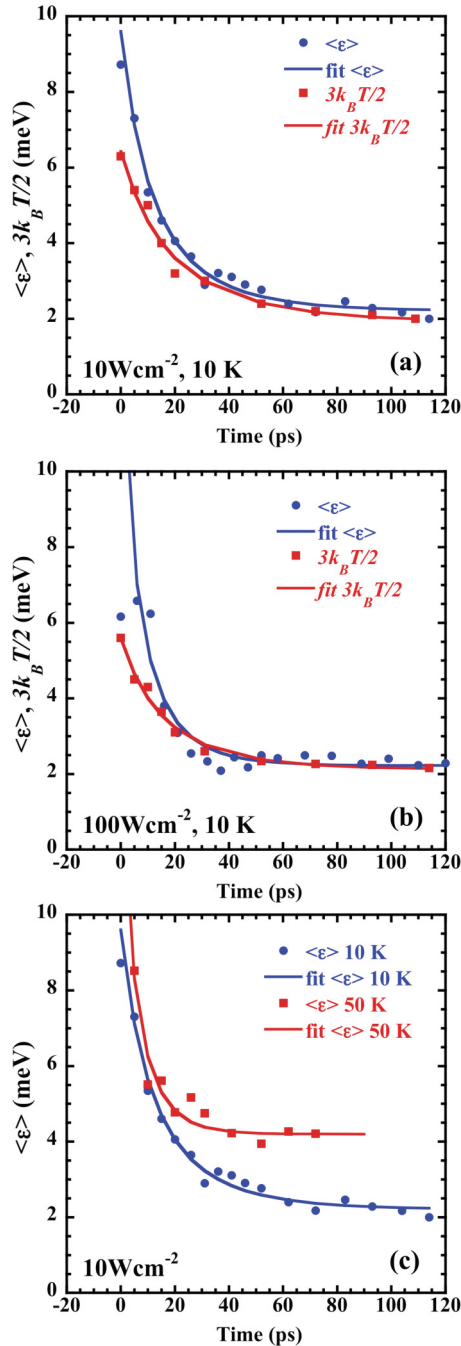


FIG. 8. (Color online) Time evolution of the exciton average kinetic energy $\langle \epsilon \rangle$ and the thermal energy along with the corresponding fits for the nonresonant excitation case (see text for details): in (a) and (b), the power density is equal to 10 and 100 W cm^{-2} , respectively, and the nominal lattice temperature amounts to 10 K. (c) Exciton average kinetic energy at two nominal lattice temperatures: 10 and 50 K for a power density of 10 W cm^{-2} . The blue curve in (c) is the same as that shown in (a). The error bars are of the order of the symbol size.

1LO-phonon emission and the 2LO-phonon band,²² while $T(t)$, according to the usual approach,¹⁴ is given by an exponential fit of the high-energy tail of the 2LO-phonon PL spectra. Obviously, for a thermal exciton distribution and a standard excitonic density of states, we expect to have

$\langle \epsilon(t) \rangle = 3k_B T(t)/2$. The two data sets, $\langle \epsilon(t) \rangle$ and $3k_B T(t)/2$, are reported in Figs. 8(a) and 8(b) for two excitation power densities. We observe that at the early stage, $\langle \epsilon(t) \rangle$ is larger than $3k_B T(t)/2$, thus denoting a nonthermal distribution of the excitons. At longer delay time, $\langle \epsilon(t) \rangle$ and $3k_B T(t)/2$ reach the same asymptotic value, as expected for an excitonic thermal distribution. In Fig. 8(c), the value of $\langle \epsilon(t) \rangle$ is reported for two different lattice temperatures $T_L = 10$ and 50 K. At $T_L = 50$ K, we see that the exciton cooling is significantly faster than that at $T_L = 10$ K. In Figs. 8(a)–8(c), the continuous lines are best fits to the experimental data obtained with the expression for the time-dependent mean energy $\langle \epsilon(t) \rangle$ [or $3k_B T(t)/2$]:

$$\langle \epsilon(t) \rangle = \langle \epsilon_\infty \rangle \left(\frac{Ae^{t/\tau} + 1}{Ae^{t/\tau} - 1} \right)^2 \quad (5)$$

with

$$A = \frac{\sqrt{\langle \epsilon_0 \rangle} + \sqrt{\langle \epsilon_\infty \rangle}}{\sqrt{\langle \epsilon_0 \rangle} - \sqrt{\langle \epsilon_\infty \rangle}}, \quad (6)$$

where $\langle \epsilon_\infty \rangle$ and $\langle \epsilon_0 \rangle$ are the equilibrium and initial (i.e., at $t = 0$) mean energy. The thermalization time constant τ is determined by the exciton-acoustic phonon interaction due to the deformation potential^{14,22} and does not depend on the lattice temperature T_L .

This expression has been very often derived assuming a thermalized distribution, therefore, it is referring to the temperature. Nevertheless, it holds independently from this assumption.¹⁷ The values determined for the time constant of $\langle \epsilon \rangle$ and $3k_B T(t)/2$ are, respectively, $\tau = 23 \pm 2$ ps and 32 ± 2 ps at 10 W cm^{-2} and $\tau = 15 \pm 1$ ps and 24 ± 1 ps at 100 W cm^{-2} ; for $T_L = 50$ K, we get $\tau = 12 \pm 1$ ps. As expected, the cooling process becomes faster when raising either the excitation power density or the temperature. In addition, the data fitting points out to a strong discrepancy between $\langle \epsilon \rangle$ and $3k_B T(t)/2$, at early times, strengthening the nonthermal distribution character of the excitonic gas.

We can now compare the energy relaxation time with the values predicted by theories. From $\tau = 23$ ps (32 ps), by means of the expression reported in Ref. 22, we get an effective deformation potential (DP) constant $E_1 = 20 \pm 1$ eV (17 ± 1 eV) to be compared with the value $E_1 = 13 \pm 1$ eV reported in Ref. 14 and $E_1 = 9 \pm 2$ eV, usually found both theoretically and experimentally (see, e.g., Ref. 23). Given that the value we find is nearly twice the “standard” one, and that the latter would lead to a thermalization time of about 100 ps, we should consider other scattering mechanisms in addition to that of the deformation potential.

A contribution to the exciton thermalization from exciton-exciton scattering is evidenced by the fastening of the initial relaxation when increasing the excitation power density from 10 to 100 W cm^{-2} , i.e., the exciton density from $\approx 10^{16}$ to $\approx 10^{17} \text{ cm}^{-3}$. In fact, the role of inelastic exciton-exciton collisions in the population redistribution in GaN has been reported by several authors.^{24,25} An evaluation of the exciton-exciton scattering rate can be obtained from the dephasing time. Indeed, according to the results of Pau *et al.* (see Ref. 26), this contribution to the linewidth depends on the exciton density N_X as $\Gamma_{XX} = \beta_{XX} a_B^3 E_B N_X$, where a_B is the exciton Bohr radius, E_B is the exciton binding energy and β_{XX} is

a dimensionless efficiency factor, which for GaN is ranging between 5 and 7. With $a_B = 3$ nm and $E_B = 24$ meV, as found from an hydrogenic model, we get a dephasing time $T_2 = \pi\Gamma_{XX}/h$ in 20 to 40 ps range for $N_X = 10^{16}$ cm $^{-3}$. We get instead a value of 2 to 4 ps for $N_X = 10^{17}$ cm $^{-3}$, which is an order of magnitude too short to account for experimental results. From our data, it turns out that, in the thermalization process, the inelastic exciton-exciton collisions contribute but with an efficiency ten times lower than in the dephasing process, where the dominant collisions do not change the energy of an individual exciton. It is also worth pointing out that the exciton-free carrier scattering process can, in principle, also contribute to the exciton relaxation but, from time-resolved spectra, given our experimental condition (temperature and excitation density) the number of free carriers seems negligible with respect to that of the excitons. In fact, a relevant contribution from uncorrelated electron-hole pairs is reported at high temperature and densities $\gtrsim 10^{18}$ cm $^{-3}$ (see Ref. 27), instead, at low temperature (10–50 K) and low excitation density ($\lesssim 10^{17}$ cm $^{-3}$), the exciton formation comes from geminate electron-hole pairs that hold the correlation in the energy relaxation process.^{28,29}

Therefore other mechanisms have to be considered and in particular the piezoelectric interaction (PZ) with acoustic phonons as well as the impurity (defects) inelastic (D^0X_A) scattering. The role of the PZ interaction in the exciton thermalization process in GaN epilayers has been extensively investigated by Kokolakis *et al.* (see Ref. 16), and it has been found nearly equal to that of the DP interaction for low residual doping. Due to screening effects, it becomes negligible for a 10^{17} cm $^{-3}$ impurity content. Since the PZ mechanism does not give a good fit to the experimental data, we consider its contribution to the thermalization as being marginal. When considering the scattering from neutral donors, the impact rate is roughly given by $\Gamma_{DX} = a_B^2 v_g N_D$,^{30,31} where N_D is the neutral donor concentration and $v_g = \sqrt{2\epsilon/m}$ is the exciton group velocity, with ϵ and m being the exciton kinetic energy and mass, respectively. Then, for example, with $\epsilon = 2$ meV and $N_D = 10^{17}$ cm $^{-3}$ we get a very short collision time $\tau_{DX} = (\Gamma_{DX})^{-1} \approx 400$ fs. Therefore even if most of the collisions are of elastic nature and they only contribute to the exciton dephasing process,³⁰ we can expect a relevant contribution to the exciton thermalization from the inelastic processes as already found in GaAs³¹ and InP.³² This mechanism is also in agreement with the observed behavior when changing the lattice temperature T_L provided the scattering rate only depends on the exciton energy and not on T_L . Thus, as observed in Fig. 8(c), the initial energy relaxation towards the exciton thermalization is independent of T_L . Since the exciton initial excess energy is identical for $T = 10$ and 50 K, the fastening of the energy relaxation observed in Fig. 8(c) is only becoming apparent as a consequence of the higher final energy of the excitons at 50 K. This does not hold for the DP (PZ) interaction. In fact, the fit of the experimental data shown in Fig. 8(c) based on Eq. (5) requires a decrease in the time constant related to the DP (PZ) interaction, when raising the temperature, in disagreement with its expression, which is independent of T_L .^{14,22}

The previous discussion deals with the time evolution of a hot-exciton population that has reached a finite and constant

value and evolves towards thermal equilibrium with the lattice. Let us now briefly comment on the early stage of the exciton dynamics when the states near the bottom of the excitonic band become populated, i.e., the exciton formation stage, which in our measurements corresponds to the time interval between the arrival of the excitation pulse and the observation of the maximum of the spectrally integrated PL of the 2LO-phonon replica [see Fig. 3(c)]. The corresponding PL rise time turns out to be ≈ 10 ps, nearly independent of the energy of the excitation photon, which is only slightly shortened when increasing the excitation power density. When exciting the sample ≈ 60 meV above the X_A state, i.e., 35 meV above the free carrier continuum, we create both free carriers and correlated e-h pairs. Free carriers relax in energy and form excitons via a bimolecular (BM) mechanism with a coefficient $B = 1.2 \times 10^{-18}$ ps $^{-1}$ cm 3 .³³ Correlated e-h pairs reach the bottom of the exciton band losing their excess energy by means of inelastic interactions with acoustic phonons, impurities, and defects. At the excitation power densities used in our experiment, the bimolecular generation only contributes at the highest power density (100 W cm $^{-2}$, i.e., 10^{17} carrier per cm 3), providing an exciton formation time of 12 ps, not far away from the observed rise time of the 2LO-phonon replica. In addition, the slight superlinearity shown in Fig. 3(c) agrees well with the BM mechanism. In our experiment at 10 W cm $^{-2}$, the exciton formation time is only slightly longer and is still in the range of 10 ps. Then it turns out to be shorter than the time needed to reach the bottom of the exciton band losing 30–40 meV of excess energy by a cascade of acoustic phonons (with an energy 2–4 meV each).¹⁶ Moreover, the BM generation would provide a rise time of ≈ 100 ps.³⁴ Therefore, also for the exciton formation, inelastic collisions with neutral donors appear as the most likely process for a fast exciton formation, or more precisely, for a fast relaxation of correlated e-h pairs towards the bottom of the exciton band. One inelastic collision, giving rise to the donor excitation/ionization, is sufficient to produce a 20–40 meV loss in the exciton energy, thus providing a fast transfer from the high-energy to the low-energy exciton states.³⁵ The fast rise in the ZPL signal, equal to that reported for the 2LO-phonon PL in Fig. 3 at low excitation power density is mainly due to exciton-impurity scattering, which avoids the bottleneck resulting from the reduced efficiency for the exciton-acoustic phonon scattering.

IV. CONCLUSIONS

From a careful analysis of low-temperature time-resolved spectra of the phonon replica emission in GaN epilayers, we have evidenced the transition from the nonthermal to the thermal regime of the exciton population. Our experimental results provide clear signatures that the processes leading to the exciton formation and thermalization are relatively slow when the exciton density is lower than 10^{17} cm $^{-3}$. The establishment of a thermal Maxwell-Boltzmann distribution for the exciton population is observed after ≈ 50 ps, mainly as a consequence of inelastic collisions with impurities rather than with acoustic phonons. From the comparison with models and predictions for the deformation potential, piezoelectric interaction, and impurity scattering, we show that scattering

with neutral donors can account for the exciton formation and relaxation. It is also concluded that the bottleneck regime for the radiative excitons at $k = 0$ is only avoided thanks to the residual doping. Nevertheless, for an exciton density $\geq 10^{17} \text{ cm}^{-3}$, exciton-exciton collisions become relevant in the exciton formation and thermalization, contributing to the cooling via inelastic processes.

ACKNOWLEDGMENTS

The research was partially supported by the Italian Ministry of University and Research PRIN “GaN optoelectronic devices for future applications: solid-state lighting, biomedical instrumentation, and data storage,” 20095NMPW7.

*vinattieri@fi.infn.it

†Also at Istituto di Fisica Applicata “Nello Carrara,” Consiglio Nazionale delle Ricerche, 50019 Sesto Fiorentino (FI), Italy.

¹A. Vinattieri, J. Shah, T. C. Damen, D. S. Kim, L. N. Pfeiffer, M. Z. Maialle, and L. J. Sham, *Phys. Rev. B* **50**, 10868 (1994).

²M. Leroux, N. Grandjean, B. Beaumont, G. Nataf, F. Semond, J. Massies, and P. Gibart, *J. Appl. Phys.* **86**, 3721 (1999).

³S. Kalliakos, P. Lefebvre, X. Zhang, T. Taliercio, B. Gil, N. Grandjean, B. Damilano, and J. Massies, *Phys. Status Solidi A* **190**, 149 (2002).

⁴S. Kalliakos, X. B. Zhang, T. Taliercio, P. Lefebvre, B. Gil, N. Grandjean, B. Damilano, and J. Massies, *Appl. Phys. Lett.* **80**, 428 (2002).

⁵B. Segall and G. D. Mahan, *Phys. Rev.* **171**, 935 (1968).

⁶C. F. Klingshirn, *Semiconductor Optics*, 3rd ed. (Springer-Verlag, Berlin, 2007).

⁷B. Gil, *Low-Dimensional Nitride Semiconductors* (Oxford University Press, New York, 2002).

⁸D. Kovalev, B. Averboukh, D. Volm, B. K. Meyer, H. Amano, and I. Akasaki, *Phys. Rev. B* **54**, 2518 (1996).

⁹I. A. Buyanova, J. P. Bergman, B. Monemar, H. Amano, and I. Akasaki, *Mater. Sci. Eng. B* **50**, 130 (1997).

¹⁰L. Cavigli, R. Gabrieli, M. Gurioli, F. Bogani, E. Feltn, J.-F. Carlin, R. Butté, N. Grandjean, and A. Vinattieri, *Phys. Rev. B* **82**, 115208 (2010).

¹¹B. Monemar, P. P. Paskov, J. P. Bergman, G. Pozina, A. A. Toropov, T. V. Shubina, T. Malinauskas, and A. Usui, *Phys. Rev. B* **82**, 235202 (2010).

¹²K. Hazu, A. Shikanai, T. Sota, K. Suzuki, S. Adachi, S. F. Chichibu, and T. Mukai, *Phys. Rev. B* **65**, 195202 (2002).

¹³T. Ishiguro, Y. Toda, S. Adachi, and S. F. Chichibu, *Phys. Status Solidi C* **6**, S719 (2009).

¹⁴D. Hägele, R. Zimmermann, M. Oestreich, M. R. Hofmann, W. W. Rühle, B. K. Meyer, H. Amano, and I. Akasaki, *Phys. Rev. B* **59**, R7797 (1999).

¹⁵K. Kyhm, L. Rota, and R. A. Taylor, *Phys. Status Solidi A* **208**, 1159 (2011).

¹⁶G. Kokolakis, F. Compagnone, A. Di Carlo, and P. Lugli, *Phys. Status Solidi A* **195**, 618 (2003).

¹⁷B. Ridley, *Quantum Processes in Semiconductors* (Oxford University Press, Oxford, 1988).

¹⁸D. Martin, J. Napierala, M. Ilegems, R. Butté, and N. Grandjean, *Appl. Phys. Lett.* **88**, 241914 (2006).

¹⁹W. Shan, R. J. Hauenstein, A. J. Fischer, J. J. Song, W. G. Perry, M. D. Bremser, R. F. Davis, and B. Goldenberg, *Phys. Rev. B* **54**, 13460 (1996).

²⁰B. Gil and O. Briot, *Phys. Rev. B* **55**, 2530 (1997).

²¹J. Shah, *Ultrafast Spectroscopy of Semiconductors and Semiconductor Nanostructures*, Springer Series in Solid-State Sciences, Vol. 115 (Springer, Berlin, 1996).

²²R. Ulbrich, *Phys. Rev. B* **8**, 5719 (1973).

²³R. Ishii, A. Kaneta, M. Funato, Y. Kawakami, and A. A. Yamaguchi, *Phys. Rev. B* **81**, 155202 (2010).

²⁴S. Bidnyk, T. J. Schmidt, B. D. Little, and J. J. Song, *Appl. Phys. Lett.* **74**, 1 (1999).

²⁵H. Tanaka, M. Ando, T. Uemura, and M. Nakayama, *Phys. Status Solidi C* **3**, 3512 (2006).

²⁶S. Pau, J. Kuhl, F. Scholz, V. Haerle, M. A. Khan, and C. J. Sun, *Phys. Rev. B* **56**, R12718 (1997).

²⁷P. Ščajev, K. Jarašiūnas, S. Okur, Ü. Özgür, and H. Morkoç, *J. Appl. Phys.* **111**, 023702 (2012).

²⁸J. Szczytko, L. Kappei, J. Berney, F. Morier-Genoud, M. T. Portella-Oberli, and B. Deveaud, *Phys. Rev. B* **71**, 195313 (2005).

²⁹K. Siantidis, V. M. Axt, and T. Kuhn, *Phys. Rev. B* **65**, 035303 (2001).

³⁰Y. J. Wang, R. X. Wang, G. Q. Li, and S. J. Xu, *J. Appl. Phys.* **106**, 013514 (2009).

³¹T. Steiner, M. L. W. Thewalt, E. S. Koteles, and J. P. Salerno, *Phys. Rev. B* **34**, 1006 (1986).

³²R. Benzaquen, R. Leonelli, and S. Charbonneau, *Phys. Rev. B* **59**, 1973 (1999).

³³S. Pau, J. Kuhl, M. A. Khan, and C. J. Sun, *Phys. Rev. B* **58**, 12916 (1998).

³⁴F. Compagnone, G. Kokolakis, A. Di Carlo, and P. Lugli, *Phys. Status Solidi A* **190**, 141 (2002).

³⁵P. P. Paskov, B. Monemar, A. Toropov, J. P. Bergman, and A. Usui, *Phys. Status Solidi C* **4**, 2601 (2007).